Carbon Nanotube Atomic Force Microscopy Tips: Direct Growth by Chemical Vapor Deposition and Application to High-Resolution Imaging

Published in *Proceedings of the National Academy of Sciences*, Vol. **97**, Issue 8, (April 11, 2000), pp. 3809–3813; doi 10.1073/pnas.050498597
 www.pnas.org/cgi/doi/10.1073/pnas.050498597

Submitted November 16, 1999; accepted January 19, 2000; published online March 28, 2000. *PNAS* version edited by Mostafa A. El-Sayed, Georgia Institute of Technology, Atlanta, GA.

Chemistry / Biophysics

Carbon nanotube atomic force microscopy tips: Direct growth by chemical vapor deposition and application to high-resolution imaging

Chin Li Cheung, Jason H. Hafner, and Charles M. Lieber*

Department of Chemistry and Chemical Biology, Harvard University, Cambridge, MA 02138
* Correspondence email: cml@cmliris.harvard.edu

Abstract

Carbon nanotubes are potentially ideal atomic force microscopy probes because they can have diameters as small as one nanometer, have robust mechanical properties, and can be specifically functionalized with chemical and biological probes at the tip ends. This communication describes methods for the direct growth of carbon nanotube tips by chemical vapor deposition (CVD) using ethylene and iron catalysts deposited on commercial silicon-cantilever-tip assemblies. Scanning electron microscopy and transmission electron microscopy measurements demonstrate that multiwalled nanotube and single-walled nanotube tips can be grown by predictable variations in the CVD growth conditions. Force-displacement measurements made on the tips show that they buckle elastically and have very small (≤100 pN) nonspecific adhesion on mica surfaces in air. Analysis of images recorded on gold nanoparticle standards shows that these multi- and single-walled carbon nanotube tips have radii of curvature of 3–6 and 2–4 nm, respectively. Moreover, the nanotube tip radii determined from the nanoparticle images are consistent with those determined directly by transmission electron microscopy imaging of the nanotube ends. These molecular-scale CVD nanotube probes have been used to image isolated IgG and GroES proteins at high-resolution.

Abbreviations: AFM, atomic force microscopy; CVD, chemical vapor deposition; SWNT, single-walled carbon nanotube; MWNT, multiwalled carbon nanotube; SEM, scanning electron microscopy; TEM, transmission electron microscopy; sccm, standard cubic centimeters per minute.

Introduction

Atomic force microscopy (AFM) has become an important technique in biology and chemistry due to its unique ability to image and characterize structures in liquid, ambient, and vacuum environments (1–4). The level of information obtained from AFM images, however, depends critically on the size, shape, and terminal functionality of the probe tips used for imaging (refs. 1–12; http://www.nanosensors.com), and whether the sample consists of isolated molecules or packed molecular arrays (6, 13). Common, commercially available AFM probes consist of microfabricated silicon or silicon nitride cantilevers with integrated pyramidal tips. These tips can have radii of curvature as small as 5 nm but are often larger, and have pyramid half cone angles of about 35° (refs. 4 and 6; http://www.nanosensors.com). The large cone angle limits the effectiveness of these tips in imaging deep and narrow features. Super sharp silicon tips with radii of curvature as small as 2–5 nm and half cone angles of about 10° have also been reported recently (http://www.nanosensors.com). However, these tips exhibit limited stability, due to brittleness of the fine silicon tip, and considerable tip-to-tip variations. An alternative approach taken for fabricating sharp and robust probes has involved depositing a spike of carbonaceous material onto the end of a regular pyramidal AFM probe (7, 8). These amorphous carbon tips have end radii of 5–12 nm and high aspect ratios (9). An advantage of these tips is that the resolution determined from images of isolated biological macromolecules reflects their radii (10–12), although the available radii and structure of amorphous carbon tips preclude detailed structural and chemically sensitive imaging of macromolecules.

To overcome these limitations of conventional tips, we have been pursuing the development of carbon nanotube probes (14–18). Carbon nanotube tips have several advantages, including (*i*) high aspect ratio for imaging deep and narrow features, (*ii*) low tip-sample adhesion for gentle imaging, (*iii*) the ability to elastically buckle rather than break when large forces are applied making them highly robust, and (*iv*) the potential to have resolution <0.5 nm in the case of individual single-walled carbon nanotubes (SWNTs) (14–21). Moreover, since nanotubes have well defined molecular structures, it should be possible using controlled synthesis to make every nanotube tip with an identical structure and resolution. If realized, this latter feature would enable nanotube probes to be characterized with a well defined transfer function similar to other structural techniques. To date, multiwalled carbon nanotube (MWNT) tips and SWNT bundle tips have been shown to image with high lateral resolution and have been selectively modified at their ends with organic and biological species to allow functionally sensitive imaging (15, 16). These studies indicate that nanotube tips will have a large impact on imaging of biological structures and macromolecular assemblies that are not amenable to current techniques such as x-ray crystallography and electron microscopy.

Nanotube AFM tips were first fabricated by direct mechanical assembly (18). In this process, micromanipulators were used to control the positions of a commercial cantilever-tip and bundle of nanotubes, while viewing with an optical microscope. This approach has allowed the initial development of nanotube tips (14–16, 18–20), although it has several significant limitations. First, the assembly procedure inherently selects toward thick bundles of nanotubes since these are easiest to observe in the optical microscope. Recently, mechanical assembly of nanotube tips also has been performed inside a scanning electron microscope (SEM) (22). The use of a SEM still limits assembly to nanotube bundles or individual nanotubes with diameters greater than 5–10 nm and, moreover, increases greatly the overall time required to make one tip. Second, well defined and reproducible tip etching procedures to expose individual nanotubes do not exist. Third, a relatively long time is required to attach nanotubes to commercial cantilevers. To overcome these limitations, we recently reported that nanotube tips could be "grown" directly by chemical vapor deposition (CVD) from commercial cantilever-tip assemblies (17). In this technique, shown schematically in Figure 1, a flattened area was created at the tip, pores were etched into the flat area, and catalyst was deposited into the pores. CVD then allowed nanotubes to grow from the tip aligned by the pores. This method produced thin, individual MWNT tips, which imaged biological structures with high resolution. CVD could ultimately be used to mass-produce tips and make them widely available. Herein, we describe detailed studies of CVD growth of MWNT and SWNT tips, the characterization of the

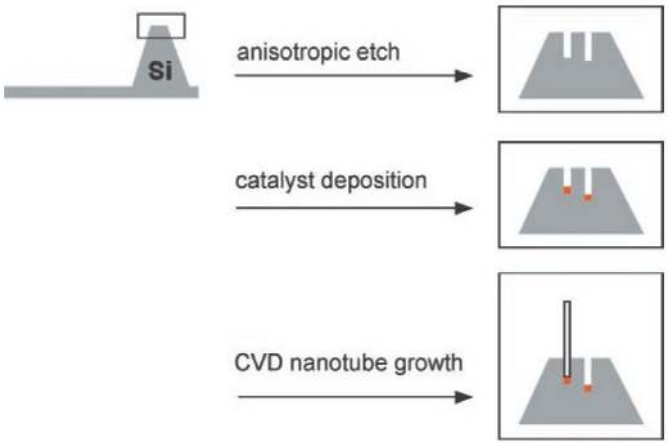

Figure 1. Schematic of the CVD nanotube tip preparation approach.

structural and mechanical properties of these tips, and high-resolution imaging of individual IgG and GroES proteins.

Materials and Methods

CVD MWNT Tip Preparation. Commercially available silicon AFM tips (Force Modulation Etched Silicon Probe, $k = 0.5–5$ N/m, Digital Instruments, Santa Barbara, CA) were flattened by scanning on silicon or CVD diamond surfaces (GE Superabrasives, Worthington, OH) in contact mode at high load (≈1 μN), high scan speed (30 Hz), and a large scan size (40 μm) for several minutes. This procedure creates a flat area of 1–5 μm^2 at the tip. Under the view of an optical microscope, the last 50 μm of the cantilever/tip assembly were placed in an ≈10-μl drop of 2.5% HF (aq) supported by two parallel grounded platinum wires acting as counter electrodes. To create ≈100-nm-diameter, 1-μm-deep pores, the tips were anodized at 2.1 V for 100 sec, were rinsed with ethanol, and then were dried in air. It is important to anodize only the end of the cantilever since the pores significantly lower its reflectivity, which can reduce signal-to-noise in AFM experiments. Anodized tips were subsequently etched in 0.03% KOH (aq) for 50 sec, were rinsed with ethanol, and were dried in air. This step removes excess silicon and opens up the pores at the surface. Iron catalyst was electrochemically deposited into the pores, under the view of an optical microscope, from an aqueous 0.01 M $FeSO_4$/0.05 M H_2SO_4 solution at –1.4 V versus the platinum counter electrodes. The tips were rinsed in ethanol to remove residual iron solution. They were oxidized in a flow of pure O_2 at 15°C/min to 600°C, were held for 20 min, and were cooled at 15°C/min to room temperature. For CVD nanotube growth, the tips were heated at 15°C/min to 800°C in a flow of 950 standard cubic centimeters per minute (sccm) argon (Ar) and 40 sccm hydrogen (H_2). At 800°C, 10 sccm of ethylene (C_2H_4) was added for 10 min, and then the furnace was cooled at 15°C/min in 1,000 sccm of Ar.

CVD SWNT Tip Preparation. SWNT tips were prepared in a similar manner to MWNT tips, except that iron oxide (FeO_x) nanoparticles were used as the catalyst. The FeO_x colloid catalyst was synthesized according to a reported method (23). A portion (0.033 moles) of $NaHCO_3$(s) was added to 50 ml of 0.0165 M $Fe(NO_3)_3$ (aq). The brick red solution was stirred vigorously for 15 min and then was diluted 1:5 times. The 1.5- to 4-nm colloidal FeO_x particles produced by this approach, which were characterized by transmission electron microscopy (TEM), were electrophoretically deposited into the pores of an HF-anodized tip at –0.5 V versus a platinum counter electrode, and then the tip was rinsed with water to remove the excess catalyst solution. CVD growth was carried out by using conditions similar to that described above for the MWNT tips. The flow rates for the H_2 and C_2H_4 were, however, reduced to 8 and 2 sccm, respectively.

Sample Preparation. Gold colloid samples with diameters of 5.7 nm (Ted Pella, Redding, CA) were used to quantify the resolution of the nanotube tips in imaging. The as-received 5.7-nm Au colloids were diluted 1:20 with deionized water. Five microliters of 1% poly-L-lysine was deposited on freshly cleaved mica for 10 sec, and then was rinsed with deionized water and dried with a stream of nitrogen. Next, 5 μl of the diluted gold colloid solution was deposited on the mica for 1 min, was rinsed with deionized water, and then was dried with nitrogen.

IgG samples were prepared from bovine IgG (>95% purity) (Sigma) by diluting to 2 μg/ml in 0.05 M PBS solution at pH 7.0. A 25-μl drop of this solution was placed onto freshly cleaved mica for 10 sec, was rinsed with deionized water, and was dried with nitrogen.

GroES samples were prepared from *Escherichia coli* GroES (>90% purity) (Panvera, Madison, WI) by diluting the lyophilized powder to 6.25 μg/ml in a 25 mM Tris buffer solution containing 75 mM KCl, 0.5 mM DTT, and 1.25% trehalose at pH 7.5. Ten microliters of this solution was dropped onto freshly cleaved mica for 10 sec, was rinsed with deionized water, and was dried with nitrogen.

AFM. All AFM images were recorded in tapping mode on a Multimode Nanoscope III or Nanoscope IIIa (Digital Instruments) in air. Free oscillation amplitudes of the cantilever were typically 10–20 nm. As-grown CVD tips are generally too long for high-resolution AFM imaging and must be shortened. The tips are shortened using a controlled electrical etching procedure (14–18). In the etching process, the nanotube tip is brought into contact with a rough niobium sample (Electron Microscopy Sciences, Fort Washington, PA) in force-calibration mode, and then a negative 5–30 V bias is applied to the sample with the tip grounded. This allows the controlled etching of the nanotubes; typically, lengths of 50–300 nm are used. Tapping mode images of the rough niobium surface can be used to evaluate qualitatively the sharpness of the tip *in situ*. Typically, the etching procedure continues until features with <10 nm are observed in the AFM image of the niobium surface.

Electron Microscopy. TEM experiments were performed with a Philips EM420 (FEI, Hillsboro, OR) operated at 100 kV. The entire AFM cantilever/tip assembly with nanotube tip was mounted on a custom TEM holder for imaging. The field emission scanning electron microscopy (SEM) images of CVD nanotube tips were obtained with a LEO 982 (LEO Electron Microscopy, Thornwood, NY) operated with a 3-kV accelerating voltage.

Results

Growth of MWNTs from a porous substrate by CVD results in nanotubes oriented perpendicular to the substrate plane (24). We have used this strategy to fabricate aligned carbon nanotube AFM tips by CVD with the proper orientation for AFM imaging. After reaction of the electrodeposited iron catalytic tips with ethylene at elevated temperature, individual multiwalled nanotubes grow from the pores etched in the flattened area at the tip. SEM images demonstrate that these nanotube tips grow in an ideal orientation for AFM imaging (Figure 2*a*). The nanotube diameters are, however, typically less than the limit of what can be accurately measured by the SEM. TEM images of the nanotube tips confirm that they are multiwalled nanotubes with well graphitized walls and radii ranging from 3–8 nm, as shown in Figure 2*b*. In addition, the as-grown nanotube tips have typical lengths of several micrometers, and are too long to be used for high-resolution AFM imaging (due to low buckling forces and low lateral stiffness). We optimize the nanotube tip length for imaging, which is typically less than several hundred nanometers, by using an electrical etching process (14, 17).

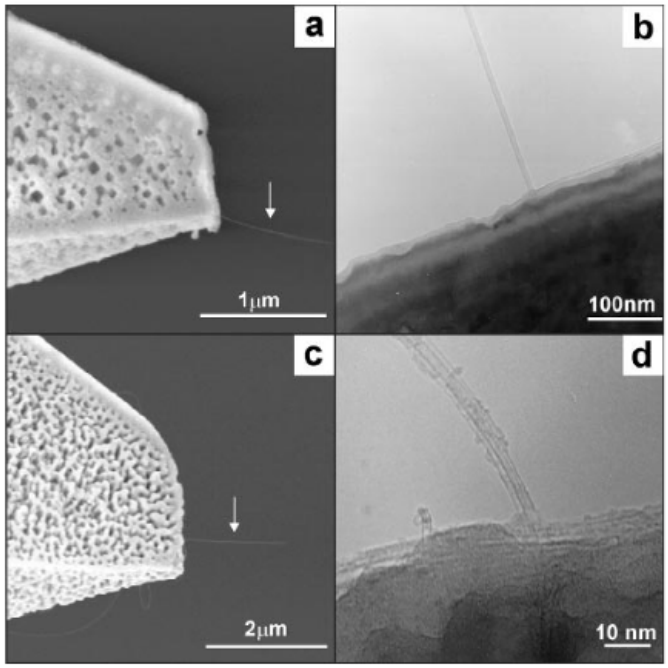

Figure 2. Electron microscopy of CVD nanotube tips. (*a*) FE-SEM image of MWNT tubes grown from a Si cantilever/tip assembly. (*b*) TEM of a CVD MWNT tip. (*c*) Field emission/SEM image of SWNT bundles grown from a Si cantilever/tip assembly. (*d*) TEM of several CVD SWNTs comprising a bundle tip.

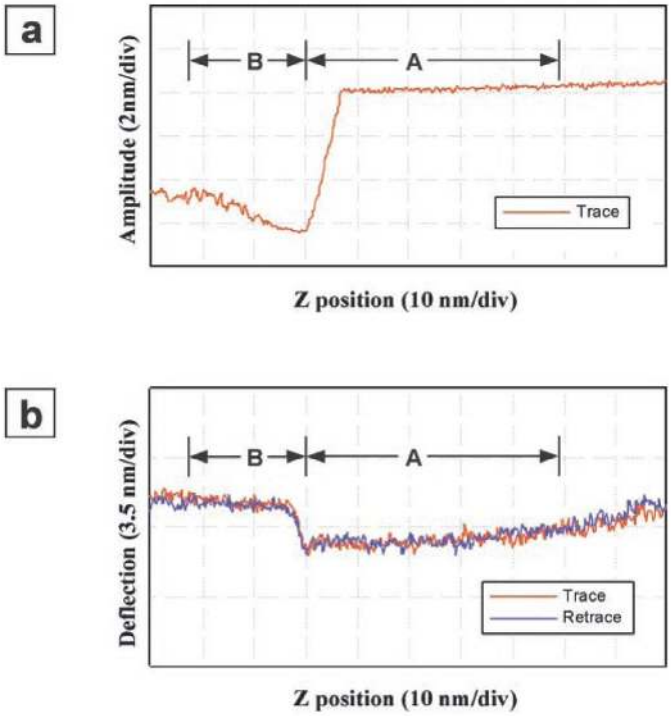

Figure 3. Force calibration plots for a CVD nanotube tip. (*a*) Tip amplitude oscillation vs. height above the sample. (*b*) Tip deflection vs. height above the sample. Regions A and B highlight the pre- and post-buckling areas.

We have also investigated the growth of SWNT tips since SWNT have the potential to produce robust probes with a resolution ≤0.5 nm. To favor the growth of SWNTs, we have used colloidal FeO_x CVD catalyst that has particle sizes comparable to the desired nanotube diameter. The gas flow was also reduced to values similar to those previously reported to favor SWNT growth in bulk catalyst powders (25). SEM images of the nanotube tips prepared by using these conditions reveal that the nanotubes grow from the tips aligned perpendicular to the flattened area and well positioned for AFM imaging (Figure 2*c*). TEM images show that these nanotubes are SWNTs, and thus demonstrate that our choice of catalyst and reaction conditions favor efficient SWNT growth from the tip ends (Figure 2*d*). Analysis of the TEM images also shows that the individual nanotubes have radii of 1–2 nm, which is comparable to the starting catalyst size, and that most of the tips consist of several SWNTs in a bundle. In the future, we believe that it should be possible to favor the formation of individual vs. bundle SWNT tips by controlling the catalyst density.

We have used the force calibration mode of the AFM to characterize the mechanics of the nanotube tips. In this mode, raster scanning is disabled so that the tip oscillates near its resonance frequency over one point on the sample. The *z*-piezo is used to bring the sample into and out of contact with the tip, while the tip oscillation amplitude and deflection are plotted versus the sample *Z* position. Typical plots obtained for a CVD nanotube tip are shown in Figure 3 *a* and *b*. Both MWNT and SWNT tips show similar characteristics. As the tip approaches (from right to left), it begins to contact intermittently the sample and the amplitude decreases as expected (region A). Upon further approach, the nanotube buckles as seen in both curves: the amplitude begins to increase again and the deflection increases to the Euler buckling force and then remains relatively constant with further approach (region B). Curves such as these have been numerically simulated for nanotube tips to confirm the nanotube-buckling behavior (18). The tip-sample adhesion can also be measured from these curves as the hysteresis in the deflection plot; it was typically found to be below the noise level of the AFM, which corresponds to a force of ≈100 pN. This is significantly smaller than that obtained with silicon tips, and can allow gentler imaging (26).

Gold nanoparticles were imaged to evaluate the resolution of CVD nanotube tips. The nanoparticles are good standards since they are well defined spherical structures and are relatively incompressible (27). As reported previously, MWNT tips produced by CVD were used to image 5.7-nm gold nanoparticles. By measuring the width of the particles in the image, the effective tip radius can be determined (6, 14). Using this technique, we find that the radii of curvature of the CVD MWNT tips were in the range of 3–6 nm, in good agreement with direct measurements of the tip size by TEM. Analysis of AFM images of gold nanoparticles taken with SWNT tips showed smaller 2- to 4-nm tip radii of curvature. This size range coincides with the SWNT bundle diameters as measured by TEM. A summary of the resolution data from both MWNT and SWNT CVD tips is shown in Table 1.

The decrease in tip radius in going from individual MWNT tips to SWNT bundle tips demonstrates the potential control and improvements in resolution that are possible with well designed catalysts. Moreover, it is quite significant that the observed image resolutions obtained with our nanotube tips are in good agreement with those expected from direct TEM measurements made on these tips. We believe that these results show that it is possible to make very high-resolution AFM probes that have predictable resolution. In addition, we note that as smaller diameter, higher resolution nanotube tips become available, the control of their length remains an important issue. Specifically, we estimate that an individual 0.5-nm radius SWNT will need to be ≤20 nm to avoid compromising the resolution due, for example, to thermal vibrations.

The small radii of curvature and low adhesion forces of nanotube tips make them ideal for imaging soft biological structures. To evaluate the potential of CVD nanotube tips in biological AFM, two proteins with known crystal structures were imaged in tapping mode:

Table 1. Summary of CVD nanotube tip resolution data

MWNT tip number	01C	20E	38A	31G	38B
Radii ± 1σ, nm	3.7 ± 0.7	4.4 ± 0.5	5.7 ± 1.7	3.2 ± 0.7	5.3 ± 0.7
SWNT tip number	51A	58B	61A		
Radii ± 1σ, nm	3.8 ± 0.7	3.0 ± 1.3	2.0 ± 0.4		

The tips are defined by a specific number and a capital letter. The number designates a particular tip and the letter the growth cycle, whereA = 1. The resolution was calculated using a two-sphere model using the full-width at half-maximum determined from the experimental images of 5.7-nm gold nanoparticles.

IgG and GroES. IgG is a 150-kDa antibody molecule that consists of four polypeptide chains arranged in a Y shape (28). Low and high-resolution images of IgG (Figure 4 *a* and *b*) show many examples of the characteristic Y shape. Because of the intrinsic conformational flexibility of IgG, we do not expect all molecules absorbed from solution to exhibit the Y shape. An indication of the high resolution obtained with these tips can be readily observed by comparing the image with the crystal structure (Figure 4*c*); that is, there is little tip-induced broadening. IgM, which consists of five IgG-like monomers arranged as a pentamer, was also imaged (17). The images clearly resolve its pentameric structure and show little broadening compared with structural models based on electron microscopy and x-ray scattering (29, 30).

GroES, which is a component of the GroEL/GroES chaperonin system involved in protein folding, is a hollow dome shaped heptamer that is approximately 8 nm in outer diameter (31). The seven 10-kDa subunits each consist of a core β-barrel with a β-hairpin loop at the top and bottom. The top β-hairpins point inward to form the top of the dome, while the bottom hairpins are disordered when not in contact with GroEL (32). Low-resolution AFM images of individual, well separated GroES molecules on mica reveal two conformations (Figure 5*a*). One conformation shows a ring-like structure with an 11-nm outer diameter and some features on the ring. The other conformation simply looks like a dome of the same diameter. We interpret these two conformations as the two sides of the GroES heptamers. The domed image is the side with the ordered β-hairpins creating the dome roof, and the ringed image is the disordered β-hairpins open to the hollow cavity. The disordered hairpins have conformational flexibility, but it is possible to observe the seven-fold symmetry, as shown in Figure 5*b* (32). For comparison, Figure 5*c* shows the bottom view of the GroES crystal structure with the top of the dome removed to make the pore visible. These results demonstrate clearly the ability of the present CVD nanotube tips to achieve submolecular resolution on isolated protein assemblies.

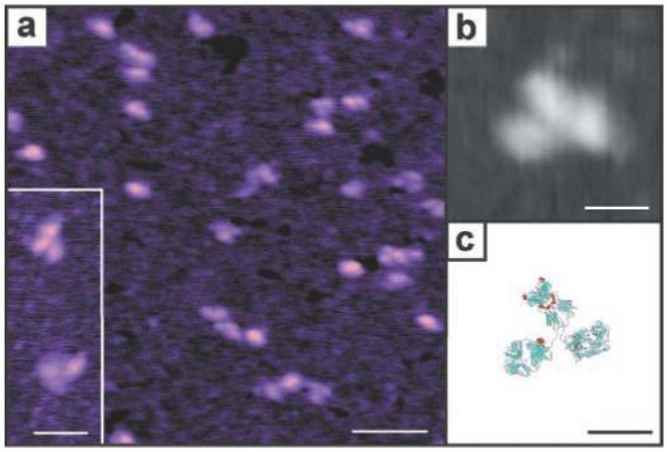

Figure 4. IgG imaged by a CVD nanotube tip. Large scan area in *a* shows several molecules that exhibit the characteristic Y shape. (*b*) High resolution images of IgG reveal very little tip-induced broadening when compared with the crystal structure in *c*. [Bars = 50 nm (*a*), 20 nm (*Inset*), 10 nm (*b*), and 10 nm (*c*).]

Discussion

We believe that the direct synthesis of carbon nanotube probes by CVD has great potential for high-resolution imaging of biological systems. By controlling the catalyst properties and CVD conditions, we have produced nanotube tips with radii of curvature down to 2 nm. Furthermore, we believe there exists a straightforward path to follow—reducing catalyst density—that will enable the growth of individual SWNT tips with radii ≤0.5 nm. The CVD method is also a key step toward putting nanotube tips into widespread use, since they can be easily grown in large quantities. More importantly, CVD allows control over the type of nanotube tip produced, which is critical for different applications. For example, if one wants a high aspect ratio tip to image trenches 1-μm deep, a relatively large diameter nanotube must be used so that the buckling

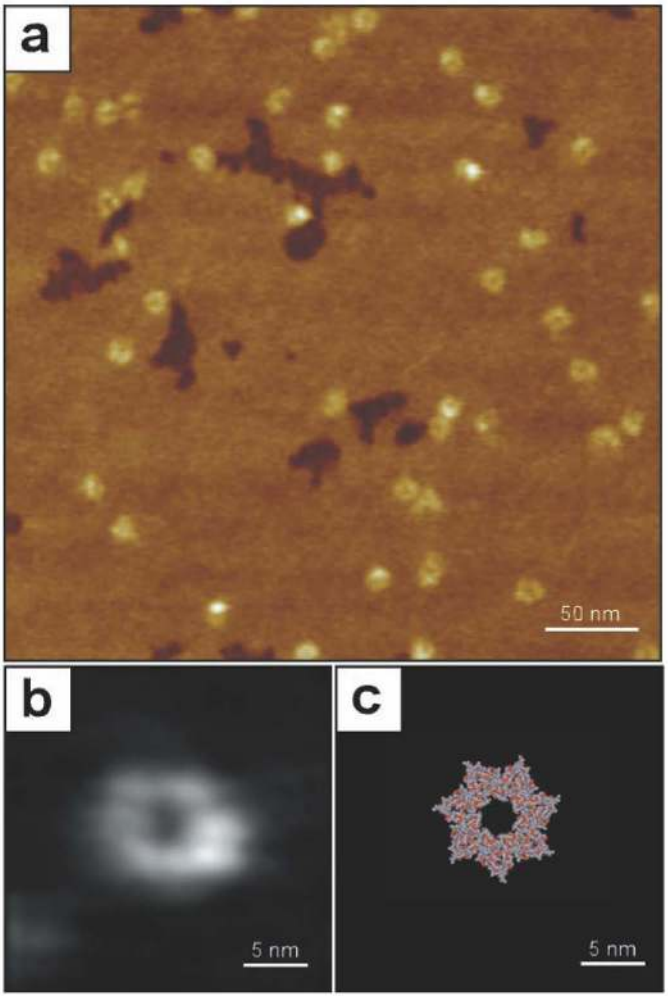

Figure 5. GroES imaged by a CVD nanotube tip. Large scan area in *a* shows both "dome" and "pore" conformations, representing the two sides of GroES facing up. (*b*) A higher resolution image of the pore side shows the heptameric symmetry, which matches well with the crystal structure (*c*).

force and thermal vibration amplitude will be acceptable. Alternatively, if one is imaging small biological structures or a membrane surface and the highest possible resolution is desired, an individual SWNT would be ideal. As we have demonstrated here, adjusting the catalyst properties and growth conditions can control the nanotube tip structure and size. This unique ability to specifically engineer nanotube tips makes CVD a powerful technique for their production and, we believe, will enable the growth of identical tips having predictable and well defined resolution in the future.

The present generation of CVD nanotube tips have demonstrated excellent imaging capabilities for biomolecules, allowing higher resolution than commercial tips and mechanically assembled nanotube tips under similar conditions. Early attempts to image IgG by AFM with commercially available tips simply showed the molecule as a featureless bump due to tip broadening (33). Shao and coworkers imaged IgG at cryogenic temperatures with commercial tips and were able to discern the characteristic Y shaped structure of IgG (34). This improvement was attributed to increased rigidity of the molecules at low temperature, which allows more stable imaging and thus higher resolution. Our IgG images clearly demonstrate that sharper tips will also enable improvements in resolution of isolated proteins at room temperature. As commercial tip production techniques have improved, they have also been used to image IgG at high enough resolution to reveal a heart-shaped structure at room temperature. However, this resolution is lower than that achieved routinely in this study.

The images of individual GroES molecules obtained with CVD nanotube tips clearly reveal the central cavity and heptameric symmetry, although the resolution is not as high as that obtained with commercial AFM tips on densely packed arrays of GroES molecules (35). Sub nanometer resolution has been reported for AFM studies of packed arrays of a number of proteins when imaged in contact mode (3, 4, 6, 35, 36). The mechanism that allows this level of resolution is not clear since similar results could not be achieved on individual molecules (36). We believe that reproducible, high-resolution imaging of individual proteins (vs. packed arrays), which is made possible with the CVD nanotube tips, is critical to many problems, including structural investigations of large protein complexes and studies of the dynamics of interacting proteins.

In addition to high structural resolution, CVD nanotube tips have the potential for high-resolution functional imaging on biological structures. Chemical modification of AFM probes allows one to differentiate between various chemical groups on a sample due to variations in the tip-sample interaction (5, 15, 16, 37, 38). In the past, modification of silicon and silicon nitride tips with monolayers has been used for chemically sensitive imaging; however, the large radii of such tips have precluded high-resolution functional mapping. We have shown recently that carbon nanotube tips can be functionalized with specific chemical and biological groups for functional imaging and force measurements (15, 16). These functionalized nanotube tips have the advantage of higher resolution and selective positioning of chemical and biological probes at the very nanotube end. In the future, we believe that modification of the new CVD tips will enable the identification of specific binding sites and chemically distinct domains of proteins.

In summary, CVD carbon nanotube AFM tips are ideal high-resolution probes for imaging biomolecules and other systems. The CVD approach to producing such tips allows great control over the tip structure and is an important first step toward making well defined, ultrahigh resolution tips, which should also be useful for functional mapping. In addition, we believe that our approach will enable nanotube tips to be made widely available to the research community.

References

1. Bustamante, C., Rivetti, C., & Keller, D. J. (1997) *Curr. Opin. Struct. Biol.* **7**, 709–716.
2. Hansma, H. G., Kim, K. J., Laney, D. E., Garcia, R. A., Argaman, M., Allen, M. J., Muller, D. S., & Parsons, S. M. (1997) *J. Struct. Biol.* **119**, 99–108.
3. Muller, D. J., Fotiadis, D., & Engel, A. (1998) *FEBS Lett.* **430**, 105–111.
4. Shao, Z., Mou, J., Czajkowsky, J., Yang, J., & Yuan, J. (1996) *Adv. Phys.* **45**, 1–86.
5. Noy, A., Vezenov, D. V., & Lieber, C. M. (1997) *Annu. Rev. Mater. Sci.* **27**, 381–421.
6. Engel, A., Schoenenberger, C., & Muller, D. J. (1997) *Curr. Opin. Struct. Biol.* **7**, 279–284.
7. Keller, D., & Chou, C. (1992) *Surf. Sci.* **268**, 333–339.
8. Akama, Y., Nishimura, E., Sakai, A., & Murakami, H. (1990) *J. Vac. Sci. Technol. A* **8**, 429–433.
9. Bustamante, C., Keller, D., & Yang, G. (1993) *Curr. Opin. Struct. Biol.* **3**, 363–372.
10. Bustamante, C., Vesenka, J., Tang, C. L., Rees, W., Guthold, M., & Keller, R. (1992) *Biochemistry* **31**, 22–26.
11. Furuno, T., Sasabe, H., & Ikegami, A. (1998) *Ultramicroscopy* **70**, 125–131.
12. Fritz, J., Anselmetti, D., Jarchow, J., & Fernandez-Busquets, X. (1997) *J. Struct. Biol.* **119**, 165–171.
13. Moller, C., Allen, M., Elings, V., Engel, A., & Muller, D. J. (1999) *Biophys. J.* **77**, 1150–1158.
14. Wong, S. S., Harper, J. D., Lansbury, P. T., & Lieber, C. M. (1998) *J. Am. Chem. Soc.* **120**, 603–604.
15. Wong, S. S., Joselevich, E., Wolley, A. T., Cheung, C. L., & Lieber, C. M. (1998) *Nature (London)* **394**, 52–55.
16. Wong, S. S., Wolley, A. T., Joselevich, E., Cheung, C. L., & Lieber, C. M. (1998) *J. Am. Chem. Soc.* **120**, 8557–8558.
17. Hafner, J. H., Cheung, C. L., & Lieber, C. M. (1999) *Nature (London)* **398**, 761–762.
18. Dai, H., Hafner, J. H., Rinzler, A. G., Colbert, D. T., & Smalley, R. E. (1996) *Nature (London)* **384**, 147–150.
19. Wong, S. S., Wolley, A. T., Odom, T. W., Huang, J.-L., Kim, P., Vezenov, D. V., & Lieber, C. M. (1998) *Appl. Phys. Lett.* **73**, 3465–3467.
20. Dai, H., Franklin, N., & Han, J. (1998) *Appl. Phys. Lett.* **73**, 1508–1510.
21. Campbell, J. K., Sun, L., & Crooks, R. M. (1999) *J. Am. Chem. Soc.* **121**, 3779–3780.
22. Nishijima, H., Kamo, S., Akita, S., Nakayama, Y., Hohmura, K. I., Yoshimura, S. H., & Takeyasu, K. (1999) *Appl. Phys. Lett.* **74**, 4061–4063.
23. Murphy, P. J., Posner, A. M., & Quirk, J. P. (1975) *Austr. J. Soil Res.* **13**, 189–201.
24. Li, W. Z., Xie, S. S., Qian, L. X., Chang, B. H., Zou, B. S., Zhou, W. Y., Zhao, R. A., & Wang, G. (1996) *Science* **274**, 1701–1703.
25. Hafner, J. H., Bronikowski, M. J., Azamian, B. R., Nikolaev, P., Rinzler, A. G., Colbert, D. T., Smith, K. A., & Smalley, R. E. (1998) *Chem. Phys. Lett.* **296**, 195–202.
26. Weisenhorn, A. L., Hansma, P. K., Albrecht, T. R., & Quate, C. F. (1989) *Appl. Phys. Lett.* **54**, 2651–2653.
27. Vesenka, J., Manne, S., Giberson, R., Marsh, T., & Handerson, E. (1993) *Biophys. J.* **65**, 992–997.
28. Harris, L. J., Larson, S. B., Hasel, K. W., & McPherson, A. (1997) *Biochemistry* **36**, 1581–1597.
29. Davos, A. C., Rous, K. H., & Shulman, M. J. (1988) *Eur. J. Immunol.* **18**, 1001–1008.
30. Perkins, S. J., Nealis, A. S., Sutton, B. J., & Feinstein, A. (1991) *J. Mol. Biol.* **221**, 1345–1366.
31. Sigler, P. B., Xu, Z., Rye, H. S., Burston, S. G., Fenton, W. A., & Horwich, A. L. (1998) *Annu. Rev. Biochem.* **67**, 581–608.
32. Hunt, J. F., Weaver, A. J., Landry, S. J., Gierasch, L., & Deisenhofer, J. (1996) *Nature (London)* **379**, 37–45.
33. Ill, C. R., Keivens, V. M., Hale, J. E., Nakamura, K. K., Jue, R. A., Cheng, S., Melcher, E. D., Drake, B., & Smith, M. C. (1993) *Biophys. J.* **64**, 919–924.
34. Zhang, Y., Sheng, S., & Shao, Z. (1996) *Biophys. J.* **71**, 2168–2176.
35. Mou, J., Czajkowsky, D. M., Sheng, S., Ho, R., & Shao, Z. (1996) *FEBS Lett* **381**, 161–164.
36. Muller, D. J., Amrein, M., & Engel, A. (1997) *J. Struct. Biol.* **119**, 172–188.
37. Frisbie, C. D., Rozsnyai, L. F., Noy, A., Wrighton, M. S., & Lieber, C. M. (1994) *Science* **265**, 2071–2074.
38. Noy, A., Sanders, C. H., Vezenov, D. V, Wong, S. S., & Lieber, C. M. (1998) *Langmuir* **14**, 1508–1511.